Journal of Fluids and Structures 28 (2012) 263–278

Contents lists available at SciVerse ScienceDirect

Journal of Fluids and Structures

journal homepage: www.elsevier.com/locate/jfs

Pressure distribution, fluctuating forces and vortex shedding behavior of circular cylinder with rotatable splitter plates

F. Gu [a], J.S. Wang [b,*], X.Q. Qiao [a], Z. Huang [a]

[a] Key Laboratory of Power Machinery and Engineering, Ministry of Education, Shanghai Jiao Tong University, Shanghai 200240, China
[b] School of Naval Architecture, Ocean and Civil Engineering, Shanghai Jiao Tong University, Shanghai 200240, China

ARTICLE INFO

Article history:
Received 18 December 2010
Accepted 10 November 2011
Available online 10 December 2011

Keywords:
Splitter plate
Vortex shedding
Fluctuating force
Suppression
Flow visualization

ABSTRACT

Previous studies on the flow around a circular cylinder with fixed splitter plates have shown that the drag and lift can be reduced, and the primary vortex shedding can be suppressed obviously. In this study, a wind tunnel experiment on the flow around a circular cylinder with diameter D (40 mm) attached with ten splitter plates freely rotatable around the cylinder axis has been carried out with different ratios of length to cylinder diameter (L/D) from 0.5 to 6.0, in a range of Reynolds number from 3×10^4 to 6×10^4. The influences of the attachment of these rotatable splitter plates on the pressure distribution, fluctuating drag and lift forces and vortex shedding behavior were investigated. It is found that the splitter plates rotate to an off-axis equilibrium angle δ (on either side of the wake with equal probability) rather than align themselves with free stream due to the integrated effect of the pressure difference along the sides of the splitter plates. The plate length L/D is crucial in determining the equilibrium angle δ. Longer splitter plate causes smaller angle; δ remains zero, i.e., parallel to the flow direction, for $L/D\geq4$. The mean pressures in the wake near the cylinder are higher than that of a bare cylinder. Further, the mean drag coefficients and the root-mean-square fluctuating lift coefficients, which are also largely determined by δ, are less than those of the corresponding bare cylinder, with a reduction up to about 30% and 90%, respectively. However, freely rotatable splitter plate develops a mean lift force towards the side the plate has deflected. In addition, the Strouhal number of fluctuating forces and correlation analysis are presented. The visualized flow structures show that the freely rotatable splitter plates elongate the vortex formation region, and the communication between the two shear layers on either side of the body is inhibited. For comparison, experiments of attaching fixed splitter plates with the same size were also conducted. The results indicate that the two kinds of splitter plates have their own advantages in force reduction and vortex shedding suppression.

1. Introduction

Unsteady flow around bluff bodies, especially circular cylinders, has been studied extensively due to the use of bluff bodies in many engineering applications, including risers in marine engineering, road vehicles, buildings, bridges, heat exchangers tubes and aircraft control. Vortex shedding in the wake can generate large unsteady forces, which have the potential to damage the structural integrity of the bluff bodies. For this reason, many methods have been proposed to

* Corresponding author. Tel.: +8602134205311.
E-mail address: jswang@sjtu.edu.cn (J.S. Wang).

0889-9746/$ - see front matter © 2011 Elsevier Ltd. All rights reserved.
doi:10.1016/j.jfluidstructs.2011.11.005

reduce lift and drag forces as well as vortex-induced structural vibrations caused by the flow over circular cylinders. Zdravkovich (1981, 1997) classified means for suppressing vortex shedding into three broad categories: (a) Disturbing the spanwise correlation with devices such as helical strakes, wires, studs or spheres, and wavy body surfaces. (b) Affecting the shear layer emanating from both sides of a bluff body with devices such as shrouds. (c) Preventing the interaction of the entrainment layers with devices such as splitter plate and base-bleed.

The rigid splitter plate was one of the earliest and most frequently used attaching suppression devices of circular cylinders. Roshko (1953), Apelt et al. (1973), Apelt and West (1975), Unal and Rockwell (1988), Texier et al. (2002), Akilli et al. (2005) and Gu et al. (2009) conducted experimental investigation on the flow patterns over a cylinder with a rigid splitter plate placed behind the cylinder. Wang et al. (2009, 2010) have studied the flow control on marine riser with attached splitter plate by numerical simulation. Roshko (1953) showed a rigid splitter plate can stabilize the near wake and suppress vortex shedding. Apelt et al. (1973) and Apelt and West (1975) investigated the effects of a rigid splitter plate placed behind a circular cylinder in a wider range of the length of the splitter plate (L). They showed that the drag coefficient and Strouhal number vary with the splitter plate length due to modifications in the near-wake flow patterns for short splitter plates ($L < 5D$) (D is the cylinder diameter). But for long splitter plates ($L > 5D$), vortex shedding is eliminated and the drag coefficient does not vary with the splitter plate length.

However, the inflow direction e.g., the current of ocean flow and the atmospheric wind direction, is variable in most real cases. Thus, a flow control device is preferred to enable the system to adapt to the different flow directions. Lam et al. (2004, 2010) investigated the fluctuating forces and vortex shedding behaviors of wavy cylinders in a cross-flow. Assi et al. (2009, 2010) used free-to rotate splitter plate, and free-to-rotate parallel plates were used to suppress VIV of a single circular cylinder and tandem cylinders. Baarholm et al. (2005) and Korkischko and Meneghini (2010) examined the effect of helical strakes with different geometric parameters on force reduction and VIV suppression. Huang (2011) tried to control the drag of fixed circular cylinders and the vortex-induced vibration of elastically supported cylinders with attaching triple-starting helical grooves.

Among these omni-directional devices, rotatable splitter plate has also drawn more attention in the recent studies. The behavior of a circular cylinder with attached splitter plate, under the conditions that the entire cylinder/splitter plate body can freely rotate around the cylinder's axis was first reported by Cimbala and Garg (1991). The entire cylinder/splitter plate body was observed to rotate to a stable position off axis. Stable splitter plate angle was plotted as a function of normalized plate length L/D. But drag and lift measurements were not provided in their work. As mentioned before, suppression of vortex-induced vibrations of a circular cylinder, with resulting drag coefficients, was achieved by Assi et al. (2009) using a free-to-rotate splitter plate. Their models were allowed to freely respond to flow-induced excitation. Their results showed that free-to-rotate splitter plates with lengths between $0.5D$ and $1.5D$ are stable. When plates outside the range were attached to the cylinder a transverse flow-induced vibration returned. As a result, the range of splitter plate lengths was chosen from $0.25D$ to $2D$. It was also found that a free-to-rotate splitter plate can reduce the drag and suppress the VIV but this configuration develops a mean transverse force. Shukla et al. (2009) studied the problem of a hinged-rigid splitter plate in the wake of a circular cylinder. The splitter plate can rotate around the hinge at the base of the cylinder rather than the cylinder axis, which is slightly different from the above two works, sustained oscillations of the hinged-rigid splitter plate occur due to the slightly different configuration.

The brief review above shows the recent work aiming to develop the flow control devices of rotatable splitter plates based on the fixed splitter plates. However, these studies are limited to a relatively narrow range of L/D, e.g., from 0.25 to 2. Furthermore, some other key parameters, such as fluctuating drag and lift coefficients for longer rotatable splitter plates, vortex shedding frequency, and correlation between two shear layers on either side of splitter plate, have not been examined. Specifically, the surface pressure distribution, which can reveal more detailed aerodynamic force characteristics, was not tested before.

The main purpose of this study is to investigate the influences on the pressure distribution, fluctuating drag and lift forces and vortex shedding behavior with attaching rotatable splitter plates to a fixed circular cylinder. A larger range of L/D from 0.5 to 6 was checked for the force and vortex shedding suppression. Different model and apparatus arrangement have been investigated in this work, and simultaneous multi-pressure measurement was first carried out, which enable the comprehensive analysis related to instantaneous aerodynamic force characteristics. Besides, smoke flow visualization was also employed as an assisted measurement to observe the flow patterns.

2. Experimental methods

2.1. Wind tunnel and experimental model

The present experiments were conducted in a 0.6×0.6 m square cross-section wind tunnel. The velocity in the test-section was controlled from 5 to 25 m/s by an inverter, resulting in a range of Reynolds numbers (based on the cylinder diameter D) from 14,000 to 66,000. The thickness of the boundary layer on the wall was measured to be about 10 mm. The free stream turbulent intensity was measured to be less than 0.1% which is sufficient to check modification of the wake structure behind bluff bodies (Gerrard (1954)). The diameter of the cylinder model in the present experiments was 40 mm with a maximum blockage ratio of 6%. By comparing the results with lower blockage ratio ($< 3\%$) models, it is found that the little differences between them can be ignored. So no attempt was made to correct the data for the blockage effect. End-plates of streamwise length $11.5D$ and width $7D$ were used, which were determined according to the results of Fox

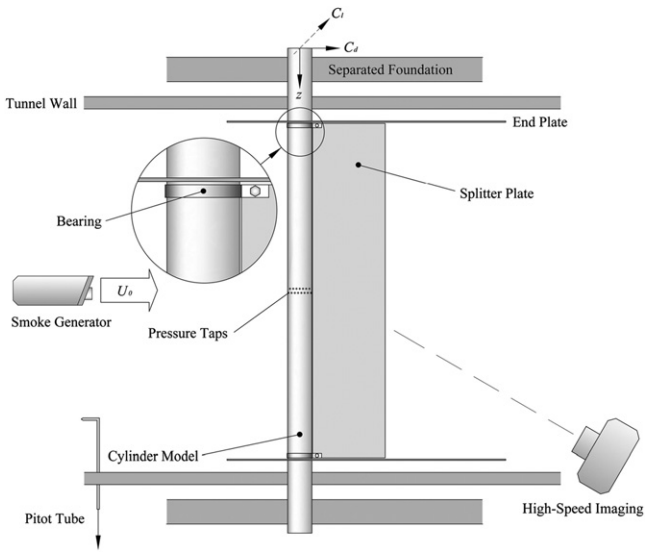

Fig. 1. Schematic diagram of the experiment setup and coordinate system.

Table 1
Length of all splitter plates.

Splitter Plates	1	2	3	4	5	6	7	8	9	10
L/*D*	0.5	1.0	1.5	2.0	2.5	3.0	3.5	4.0	5.0	6.0

and West (1990). The aspect ratio of the cylinder between the plates was 12.5, which is large enough to ensure the presence of a region of two-dimensional flow conditions over a central portion of the span (Szepessy and Bearman (1992)).

A schematic diagram of the experiment setup and coordinate system used in this study is shown in Fig. 1. The cylinder was vertically mounted in a built-in support so that the influence of the gravity can be ignored during the process of the motion of the splitter plate. Two ball bearings ($30 \times 42 \times 7$ mm) were installed at both ends of the cylinder to make them freely rotatable around the cylinder axis. The bending stiffness and damping associated with the bearings were so small that they are unlikely to influence the dynamics. Then two clamps were used to fix the splitter plate to outer ring of the bearings. About 1 mm gap between splitter plate and cylinder was left to avoid friction. The splitter plates were made of a rigid Aluminum sheet of 0.05*D*. The effective stiffness of the plates was measured to be sufficient to resist bending of the plates, so rotations were purely due to the bearing. It has been proven by Assi et al. (2009) that the torsional resistance resulting from friction in the bearings holding the plates plays a significant role in the dynamics of the splitter plate. The torsional friction would lead to severe oscillations if it is below some critical value and presumably would result in galloping oscillations if it is too large. The torsional resistance (τ_f) of the present apparatus has been determined to be 0.043 Nm per unit length of the cylinder, which is between the critical value 0.025 Nm/m and the upper threshold 0.055 Nm/m. It is sufficient to suppress vibration. The nondimensional friction torque parameter τ_f^*(defined as $\tau_f/\rho U^2 D^2$) of the present experiments are also in the plate-stable level as suggested by Assi et al. (2009).

The lengths of all the ten splitter plates used in the present experiments are shown in Table 1. For comparison, experiments of attaching fixed splitter plates with the same lengths along the streamwise direction were also conducted.

2.2. Simultaneous multi-pressure measurement and flow visualization

Because the rotatable splitter plate was installed separately from the cylinder, which was different from the entire cylinder/splitter plate body of the work of Cimbala and Garg (1991), pressure taps can be set around the surface of the cylinder. As a result, the present experiments could be conducted using a self-developed simultaneous multi-pressure measurement system. The system consists of 30 pressure sensors (Honeywell DC010NDC4) and 64-channel analog input card (Advantech PCI-1747U) acquisition system.

Thirty pressure taps were set and evenly distributed around the surface of the central section of the cylinder in two rows (the spacing between two neighboring taps was 12°). The gap between the two rows was small enough to be recognized as a uniform two-dimensional cross-section. The diameter of the tap hole was 1 mm. A short stainless steel tube was inserted tightly into each tap hole and then connected to a polyurethane tube. The length of the steel tube was 8 mm, and its inner and outer diameter was 0.8 mm and 1 mm, respectively. The length and inner diameter of the

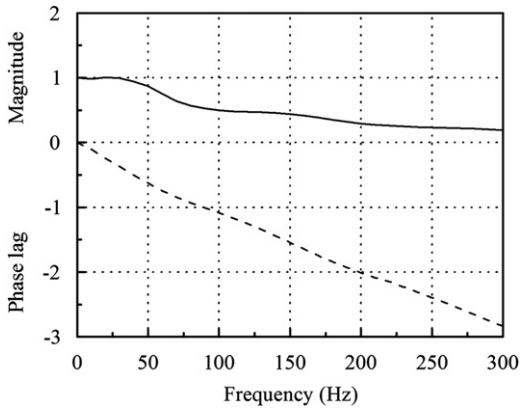

Fig. 2. Magnitude and phase lag of the transfer function of the tubing combination.

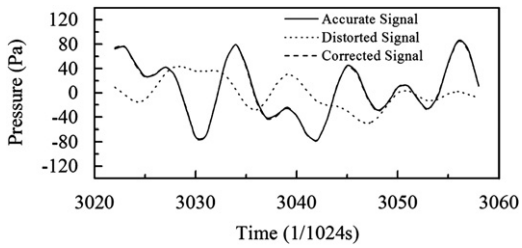

Fig. 3. Effect of the correction.

polyurethane tube was 1100 mm and 1 mm, respectively. Pressure signals were transmitted to individual pressure sensors through the tubing combination. Distorted pressure signals through the pressure transfer tubing combination were corrected with the method provided by Irwin et al. (1979). Tests were undertaken so as to establish the transfer function for the tubing combination. The magnitude and phase lag of the transfer function are shown in Fig. 2. The frequency range of the measurements was chosen from 0 to 300 Hz, covering all the frequencies of interest. To verify the reliability of the transfer function, a test correction was done. Firstly, a fluctuating pressure was generated by a public address horn. The horn was driven by a power amplifier whose signal was driven by a program controlled D/A card. The fluctuating pressure signal was composed of several sinusoidal signals with different frequencies, magnitudes and phases. The measurement system was used to capture two sets of the fluctuating pressure data. One was captured by the sensor directly; the other was captured through the above-mentioned transfer tubing combination to the sensor. So the first set of data could be recognized as accurate signal. The second set of data would be the distorted signal that needs correction. Fig. 3 shows the two signals with the corrected signal. It is evident that the corrected signals are in a good agreement with the accurate signal. The root-mean-square error and correlation coefficient between the two were 2.85 Pa and 0.9939, respectively, which meets well the accuracy.

The data acquisition system has a high resolution of 16 bits and sampling rate up to 250 kS/s, which guarantees simultaneous pressure measurement. The data from each sensor was simultaneously sampled at a rate of 1024 S/s. On the other hand, program module to eliminate the influence of drift and zero offset from the experimental data was also written into the acquisition system.

The smoke flow visualization technique was employed to help explain the differences in fluctuating forces with detailed flow structures. A smoke generator was placed in front of the settling chamber of the wind tunnel. A high-speed imaging system (PHOTRON FASTCAM ultima APX-i2) was used to obtain clear images of the turbulent wake. Full 1024×1024-pixels image resolution and 2000 fps imaging speed were chosen in the experiments.

3. Results and discussion

According to the wind speed provided by the wind tunnel, the experiments were performed at four Reynolds numbers, 3×10^4, 4×10^4, 5×10^4, and 6×10^4.

3.1. Dynamic equilibrium positions for the rotatable splitter plates

As shown in Fig. 4, angle of the circumference θ was measured from the time-averaged stagnation point. Side A and side B are designated respectively as $\theta < 180^\circ$ and $\theta > 180^\circ$. The present study shows that rotatable splitter plates oscillate

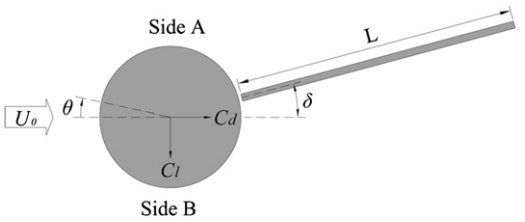

Fig. 4. Schematic diagram of angle of the circumference θ and equilibrium offset angle δ.

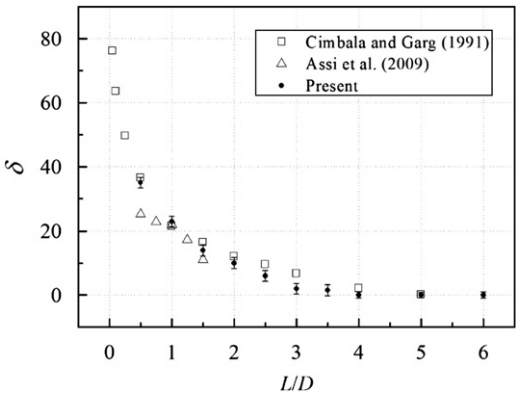

Fig. 5. Equilibrium offset angle δ versus L/D.

slightly with very small amplitude in some certain equilibrium position. The displacement amplitude parameter A (defined as the displacement of plate-tip in the transverse direction) was below $0.05D$ for each plate.

It was observed that there are three dynamic equilibrium positions for the short rotatable splitter plates, two stable and one unstable. The two stable equilibrium positions are symmetrical to the centerline due to two-dimensional flow conditions. If the splitter plate was not placed at equilibrium position, it would rotate under the integrated effect of the pressure difference between both sides of the splitter plate from the initial position to the nearest stable equilibrium position very soon. But if it was placed just right at the unstable equilibrium position $\theta=180^\circ$, splitter plate would stay still for a period of time until any disturbance strong enough to break the dynamic equilibrium state occurs, after that the splitter plate would also rotate to either of the stable equilibrium position. The behavior was also reported by Cimbala and Garg (1991) and Assi et al. (2009), but no clear explanation of the behavior was given. However, it is reasonable to believe that the unstable moment caused by the unsteady flow is responsible for this behavior. The time-averaged flow in the separated near wake of the cylinder imposes a nonzero unstable moment about the axis on the splitter plate, forcing it assembly to rotate to one of the two stable positions where the moment are zero.

Different behaviors were observed for the long plates ($L/D \geq 4.0$). The two equilibrium positions are so close that splitter plate would oscillate slightly ($A < 0.1D$) at $\theta=180^\circ$instead of deflecting to a stable angle on one side. Stable positions were found outside the stable range $0.5D$ to $1.5D$ observed by Assi et al. (2009). This behavior may be because the present system was not allowed to respond to flow-induced excitation. As discussed before, a secondary effect might be the level of torsional friction. Thus it can be regarded that there is only one equilibrium position for the long rotatable splitter plates. Equilibrium offset angle δ, the absolute value of the difference between $\theta=180^\circ$ and equilibrium angle, was found to be independent of Reynolds number for the range tested. It was read on an angle dial which was stuck on the end plate below. These angles at $\mathrm{Re}=5\times10^4$ are plotted with error bars in Fig. 5 as a function of normalized plate length L/D along with results from Cimbala and Garg (1991) and Assi et al. (2009). It can be seen that, longer splitter plate causes smaller equilibrium offset angle; δ remains zero, i.e., parallel to the flow direction, from $L/D=4$. The current results are in good agreement with the results of other researchers. It is also found that the equilibrium offset angle is almost independent to Reynolds number in sub-critical regime which implies that the moment is caused primarily by pressure rather than viscous forces.

3.2. Mean and fluctuating pressure distribution

3.2.1. Mean pressure distribution

Fig. 6 shows the mean pressure distributions of the bare cylinder at different Reynolds numbers. The flow states are not sensitive to the Reynolds number, because the present experiments are carried out in sub-critical flow. The present experiments were validated by the bare cylinder results of Cantwell and Coles (1983), Fage and Falkner (1931) and, as well as Weidman (1968). For this reason, the paper will only discuss mean pressure distributions at $\mathrm{Re}=5\times10^4$.

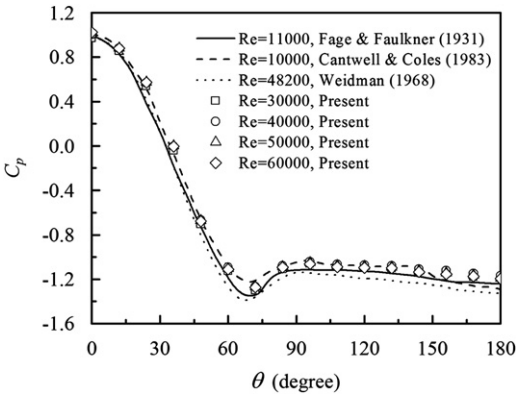

Fig. 6. The mean pressure distributions of bare cylinder at four Reynolds numbers.

Due to symmetry of the two equilibrium positions on both sides for rotatable splitter plates, only side A is discussed hereinafter. Fig. 7 (a) and (b) show the mean pressure distributions for fixed and rotatable splitter plates attached, respectively. In the figures, $L/D=0$ stands for circular cylinder without any attachment, where $C_p$has a minimum value at about $\theta=72^\circ$ (symmetrically at $\theta=288^\circ$). The inflection point was at about $\theta_s=86^\circ$, which is considered to be the time-averaging separation angle in accordance with the recommendation of Zdravkovich (1997). The base pressure C_{pb} (that is at $\theta=180^\circ$) which is obviously minimal in near wake is -1.220. As for the long rotatable plates ($L/D\geq 4.0$, the same below), the results of rotatable splitter plates are similar to fixed ones. But for the short ones ($L/D\leq 3.5$, the same below), the mean pressure distribution is no longer symmetrical to $\theta=180^\circ$. On both sides of the plate, flow separation took place at different angles for different splitter plates, but it is evident that both of them moved slightly forward to stagnation point direction as a result of the compression of flowing space caused by the splitter plate. It is in agreement with the mean steady lift observed by Assi et al. (2009). There is a jump in pressure in the stable position (θ_e), but there has to be zero moment acting on the plate. Hence further along the plate there has to be a substantial rise in pressure on the side away from the wake center line. It indicates that on the side to which the plate deflected the separating shear layer from the cylinder reattaches to the tip of the plate and this has the effect of stabilizing the near wake flow. For the long plates, near wake pressure distribution on each side of the plate remains stable, which is different from that of the corresponding circular cylinder where there is an obvious dip at $\theta=180^\circ$, because the two shear layers on either side of the body were split by the splitter plate. The communication between them is inhibited to some extent. There was no fully developed vortex street in the wake near the body, so the flow intensity was reduced and there is no obvious jump in pressure at their base.

Different splitter plate lengths result in different mean surface pressure distributions. But the differences of C_p increment compared to the corresponding circular cylinder between different length plates are bigger than that of fixed plates. To show the effect of splitter plate length on the C_p in near wake, three average values of C_p are presented in Fig. 8. $\overline{C}_{p,\,A}$ and $\overline{C}_{p,\,B}$ are the average values from $\theta_{s,\,A}$ (separation angle at side A) to θ_e and from θ_e to $\theta_{s,\,B}$ (separation angle at side B) respectively, while $\overline{C}_{p,\,wake}$ is the average value of the entire near wake. It is evident that the three values increased almost linearly with increasing L/D from 0.5 to 4.0, but $\overline{C}_{p,\,wake}$ became nearly unchanged for $L/D\geq 4.0$.

3.2.2. Fluctuating pressure distribution

The fluctuating pressure coefficient C'_p against θ is plotted for attaching fixed splitter plates under different plate length in Fig. 9 (a) and (b) (Fig. 9(b) shows the local amplified results without bare cylinder for a clear view). For bare cylinder, C'_p reaches a maximum of 0.420 at separation point $\theta_s=86^\circ$ and a second peak of 0.361 at about $\theta=144^\circ$. It agrees with the results of Nishimura and Taniike (2001) and Norberg (2003).

For attaching fixed splitter plates cases, fluctuating pressure distributions are similar. Due to the suppression of vortex shedding near the cylinder, C'_p is much less than that of bare cylinder. The separation points are all around $\theta_s=84^\circ$, and there are second peaks at about $\theta=140^\circ$. The shear layers separated from the cylinder cannot develop into vortices at $\theta=180^\circ$ because the plate stops communication between the two shear layers and inhibits instability, so C'_p is reduced to near the value at the stagnation point.

Fig. 10(a) and (b) illustrate the fluctuating pressure distribution of attaching rotatable splitter plates. By comparing Fig. 9 and Fig. 10, there are apparent offsets in fluctuating pressure distributions to the direction of increasing θ. The separation points and the second peak points also increase. C'_p at $\theta>180^\circ$ is bigger than the corresponding position at $\theta<180^\circ$. According to the analysis, that is because compression to the shear layer caused by splitter plate on side A is stronger than on side B. Shear layer on side B has more development space, which is beneficial to vortex formation. Therefore stronger flow on side B leads to larger fluctuating forces.

Regardless of fixed or rotatable splitter plates, fluctuating pressure distribution varies with plate lengths. Fig. 11 reveals C'_p at separation point versus L/D. The two separation points at side A and B for rotatable splitter plates are not symmetrical, so the two C'_p values are both presented. C'_p is the biggest at $L/D=0.5$. With the increase of L/D, C'_p drops to

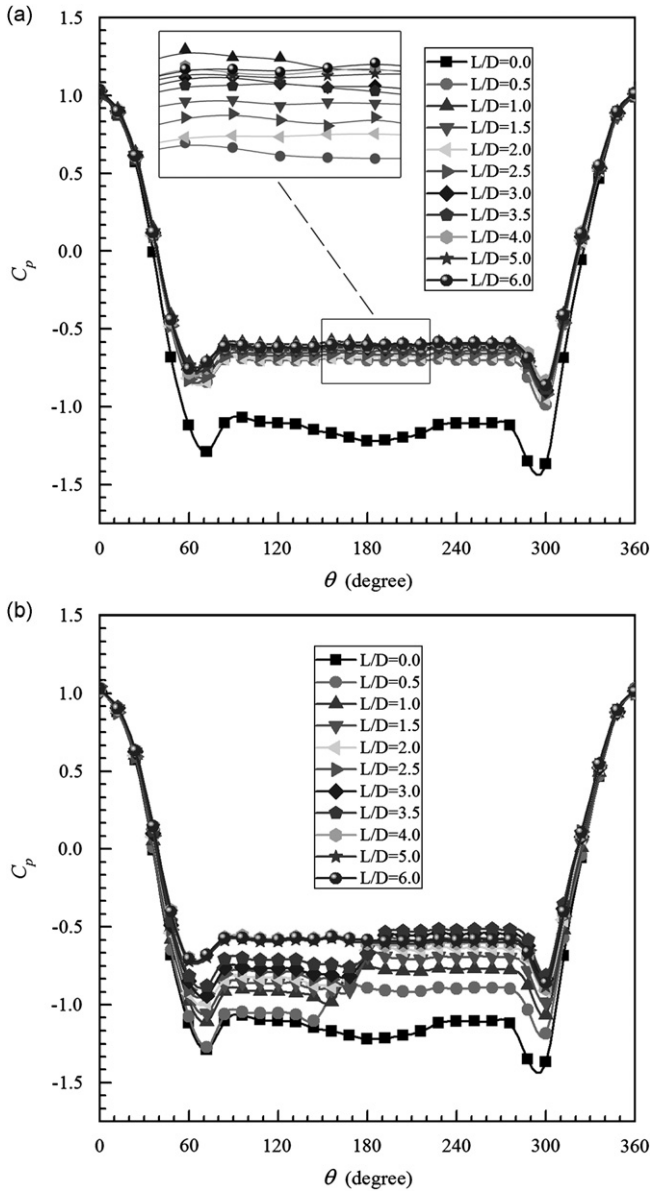

Fig. 7. Mean pressure distributions for fixed (a) and rotatable (b) splitter plates attached.

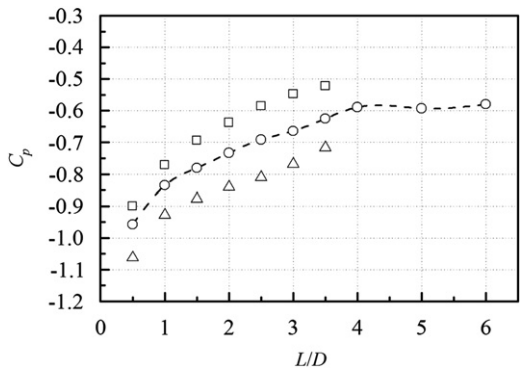

Fig. 8. Average pressure in the wake near cylinder versus L/D. Key: □, $\overline{C}_{p,\,A}$; △, $\overline{C}_{p,\,B}$; ○, $\overline{C}_{p,\,wake}$.

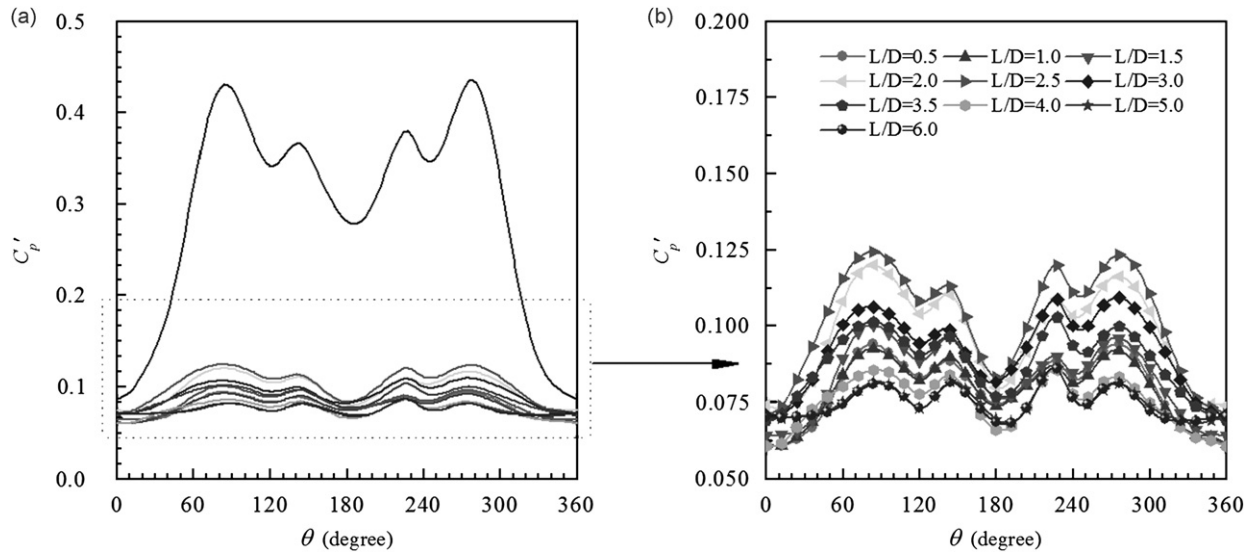

Fig. 9. The fluctuating pressure coefficient C_p' plotted against θ of fixed splitter plates.

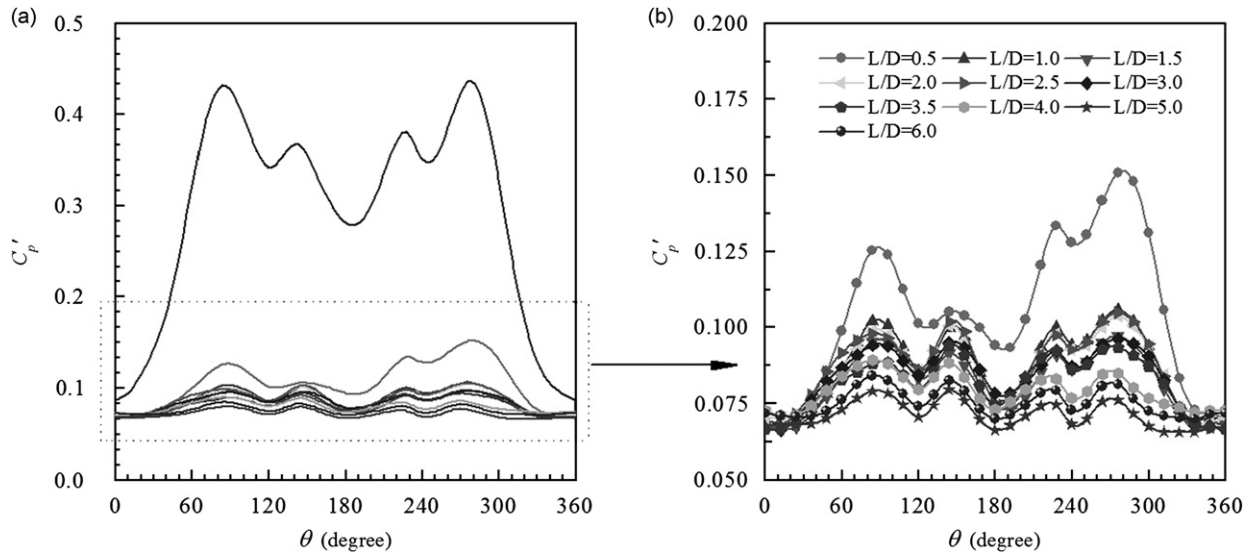

Fig. 10. The fluctuating pressure coefficient C_p' plotted against θ of rotatable splitter plates.

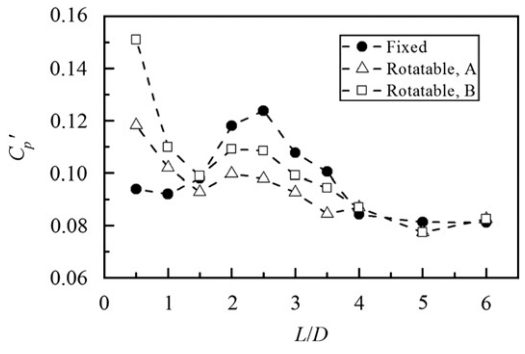

Fig. 11. The fluctuating pressure coefficient C_p' at separation point versus L/D.

less than 0.10 at $L/D=1.5$ and rises again till $L/D=2.5$. After that, C_p' decreases slowly until $L/D=6.0$. Comparison between fixed and rotatable plates indicated that $L/D=1.5$ and $L/D=4.0$ are two turning points. C_p' of rotatable plates are larger than fixed ones when $L/D<1.5$. It is opposite when $1.5<L/D<4.0$. But they are almost equal when $L/D\geq 4.0$.

3.3. Mean and fluctuating forces coefficient

Fluctuating pressure distributions were integrated to acquire the time series of fluctuating lift and drag. Mean drag coefficient C_d versus Re for a circular cylinder is plotted together with the results of Wieselsberger (1921) and Zdravkovich (1997), which are fairly accurate and widely adopted, in Fig. 12. It can be seen that the two sets of data are in good agreement with each other. Therefore, it can be concluded that the test and processing method used are fairly reliable.

The mean and fluctuating drag coefficient of attaching fixed and rotatable splitter plates at the four Reynolds numbers are shown in Figs. 13 and 14, respectively. In the figures, solid symbols represent fixed splitter plates while the corresponding hollow symbols represent rotatable cases (hereinafter the same). It can be observed that the C_d and C_d' of both fixed and rotatable cases are less than those of the bare cylinder. Like mean pressure coefficient, mean drag coefficient is almost independent of Reynolds number. However, L/D is an important parameter to control mean drag coefficient. C_d of the short rotatable splitter plates are higher than that of the corresponding fixed ones while C_d of the long plates are roughly equal. Besides, there is a steady decrease of C_d from $L/D=0.5$ to 3.5 for rotatable cases, but it twists and turns for fixed cases. It is not difficult to find that $\overline{C}_{p,\,\mathrm{wake}}$ and C_d show an opposite trend with the increase of L/D by comparing Figs. 8 and 13. The mean drag C_d is due to the influence of the downstream side, because the pressures of upstream side in all cases are almost the same. For comparison, results of free-to-rotate splitter plates from Assi et al. (2009) were also plotted in Fig. 13. The variation trends of C_d from $L/D=0.5$ to 1.5 are similar, and the values at $L/D=1$ are almost equal. The values at $L/D=0.5$ and 1.5 of Assi et al. (2009), however, are slightly smaller than that of the present work. Compared to Fig. 5, the differences of C_d between Assi et al. (2009) and the present are similar to that of the equilibrium offset angle δ. It illuminates that the equilibrium offset angle is a determinant factor of the C_d of attaching rotatable plates while the differences of δ between the two works may be due to the different supporting methods of models, experimental facilities and fluids.

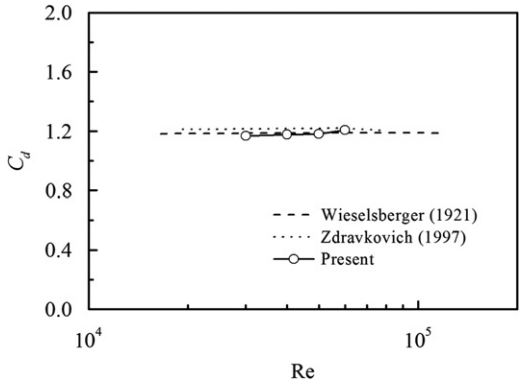

Fig. 12. Mean drag coefficient C_d for a circular cylinder as a function of Re.

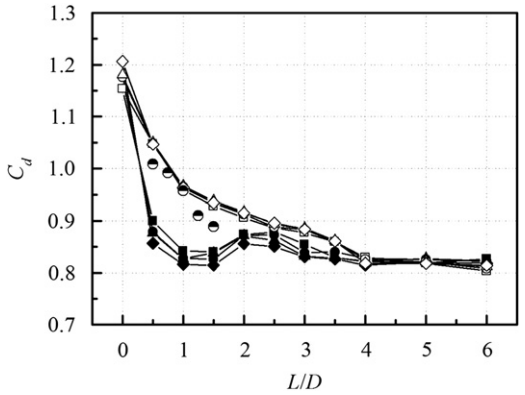

Fig. 13. The mean drag coefficient of attaching fixed and rotatable splitter plates at the four Reynolds numbers. Key: ■, fixed at $\mathrm{Re}=3\times10^4$; ●, fixed at $\mathrm{Re}=4\times10^4$; ▲, fixed at $\mathrm{Re}=5\times10^4$; ▲, fixed at $\mathrm{Re}=6\times10^4$; □, rotatable at $\mathrm{Re}=3\times10^4$; ○, rotatable at $\mathrm{Re}=4\times10^4$; △, rotatable at $\mathrm{Re}=5\times10^4$; ▲, rotatable at $\mathrm{Re}=6\times10^4$; ◓, results of free-to-rotate splitter plates from Assi et al. (2009) at about $\mathrm{Re}=3\times10^4$.

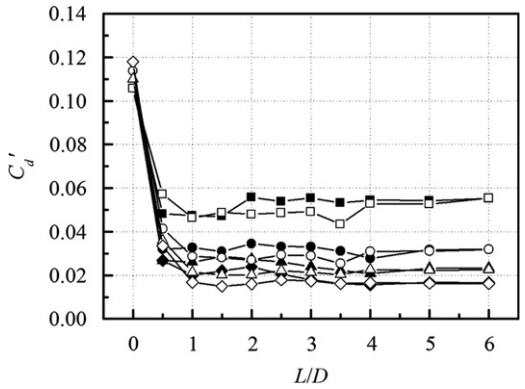

Fig. 14. The fluctuating drag coefficient of attaching fixed and rotatable splitter plates at the four Reynolds numbers. Key: the same as Fig. 13.

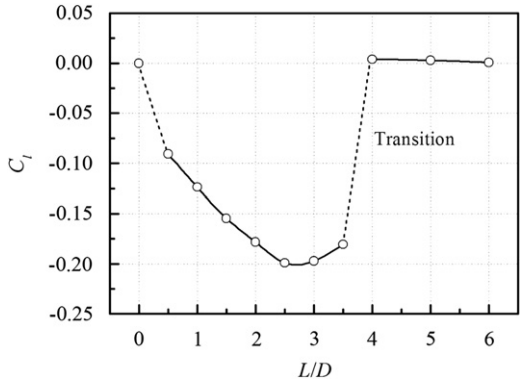

Fig. 15. The mean lift coefficient of rotatable plates plotted against L/D at $\mathrm{Re}=5\times10^4$.

For fluctuating drag coefficient, L/D is no longer a determinant parameter. However, C_d' goes down with the rise of Reynolds number. C_d' of the short rotatable splitter plates are lower than that of the corresponding fixed ones except $L/D=0.5$.

As mentioned by Assi et al. (2009), free-to-rotate splitter plates develops a mean lift force towards the side the plate has deflected. The mean lift coefficient of rotatable plates are plotted against L/D at $\mathrm{Re}=5\times10^4$ (similar at other three Reynolds numbers) in Fig. 15. There is a maximum C_l absolute value of 0.199 when $L/D=2.5$. A dramatic drop of lift to zero occurs at the transition region between $L/D=3.5$ and 4.0. Fig. 16 shows the fluctuating lift coefficient versus L/D at the four Reynolds numbers. It can be seen that the variation trend of C_l' towards L/D are similar between fixed and rotatable splitter plates, but the magnitude of variation for rotatable cases is smaller.

Mean drag (C_d) and fluctuating lift (C_l') coefficients of rotatable splitter plates and their percentage reduction relative to bare cylinder at $Re=5\times10^4$ are tabulated in Table 2. Within the studied range of $0.5\le L/D\le6.0$, a maximum mean drag and fluctuating lift reduction of up to 31% and 91% was obtained when $L/D=6.0$ Fig. 16.

3.4. Spectral analysis

The power spectral density (PSD) is used to reveal the frequency domain features of vortex shedding. The PSD distributions of fluctuating lift for $L/D=0$, 1.5, 2.5 and 5.0 are shown in Fig. 17 (Note the different vertical coordinate dimensions for each case). The results show that the plate length is a major factor that influences the variation of the Strouhal number (St) while Re has little effect. Thus, only power spectral density at $\mathrm{Re}=5\times10^4$ is discussed. In other words, the plate length affects remarkably upon the formation of vortex shedding behind the cylinders. It is found that there is only one clear and distinct peak frequency for $L/D<4$ plates, but two extremely weak peak frequencies for $L/D\ge4$ plates, which means that the energy of the vortex street is very weak or the vortex shedding is very steady at these cases.

Fig. 18 is the plots of St and its corresponding log PSD versus L/D, respectively. It indicates that the shedding frequency is higher than that of a bare cylinder when $L/D\le2$ but gets lower than that when $L/D>2$. St decreases from 0.226 to 0.148 with increasing L/D from 0.5 to 3.5. Due to the different equilibrium situation, St increases up to about 0.17 suddenly between $L/D=3.5$ and 4.0, and a second peak frequency appears. The spectral power at St for short splitter plates is much lower than bare cylinder which means vortex shedding is inhibited to some extent. There are two extreme values at $L/D=1.5$ and 2.5. The observed trend explains the impact of vortex shedding intensity on the fluctuating lift of L/D.

Table 2
Mean drag and fluctuating lift coefficients of rotatable splitter plates and their percentage reduction relative to bare cylinder at $Re=5\times10^4$.

	L/D	0.0	0.5	1.0	1.5	2.0	2.5	3.0	3.5	4.0	5.0	6.0
Fixed	C_d	1.180	0.877	0.827	0.838	0.871	0.862	0.832	0.829	0.823	0.827	0.823
	Reduction		25.71%	29.90%	28.98%	26.17%	26.94%	29.49%	29.77%	30.30%	29.88%	30.28%
	C_l'	0.468	0.067	0.055	0.080	0.131	0.133	0.118	0.099	0.066	0.046	0.043
	Reduction		94.28%	95.37%	93.21%	88.88%	88.73%	90.02%	91.64%	94.39%	96.10%	96.39%
Rotatable	C_d	1.180	1.050	0.967	0.938	0.917	0.894	0.886	0.862	0.818	0.821	0.812
	Reduction		11.03%	18.09%	20.50%	22.28%	24.28%	24.96%	26.93%	30.66%	30.43%	31.22%
	C_l'	0.468	0.140	0.099	0.089	0.106	0.110	0.098	0.080	0.065	0.044	0.040
	Reduction		70.10%	78.79%	80.97%	77.34%	76.40%	79.10%	82.91%	86.11%	90.66%	91.38%

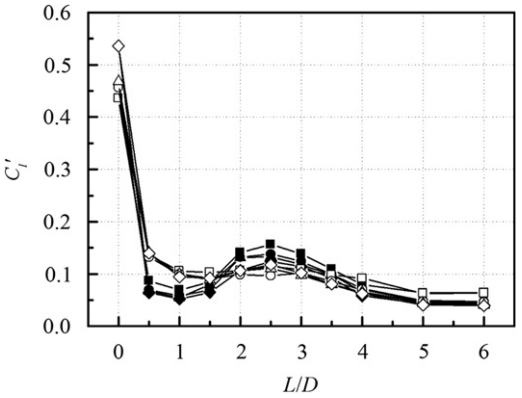

Fig. 16. The fluctuating lift coefficient versus L/D at the four Reynolds numbers. Key: the same as Fig. 13.

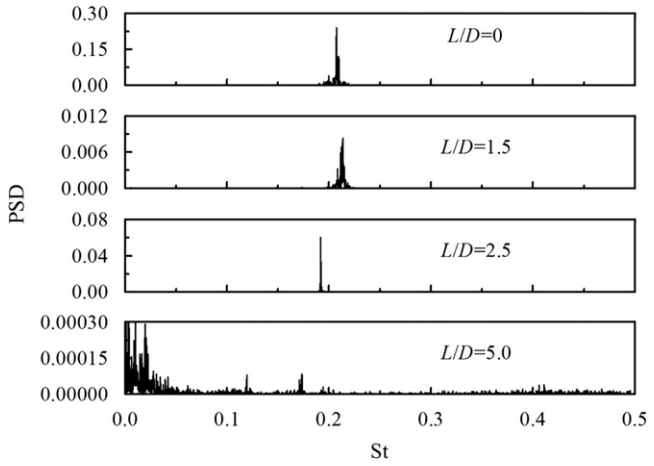

Fig. 17. The PSD distributions of fluctuating lift for splitter plates ($L/D=0$, 1.5, 2.5 and 5.0).

The situation for long splitter plates is different in that the PSD values of the two peak frequencies are very low and almost no vortex develops in the near wake.

Gerrard (1966) suggested that the frequency of vortex shedding is proportional to the length scale of the vortex formation region immediately downstream of the body. This is verified by the flow visualizations and, hence, discussed later in this paper.

3.5. Correlation analysis

Correlation analysis can reveal implicit periodicity of signals and detect degree of correlation between two signals. The correlation between fluctuating lift and pressures on circumferential surface of the cylinder ($\tilde{R}_{lp(\theta)}$) was analyzed–as well as the correlation of pressure at separation point and fluctuating pressures on circumferential surface of the cylinder ($\tilde{R}_{p(s)p(\theta)}$).

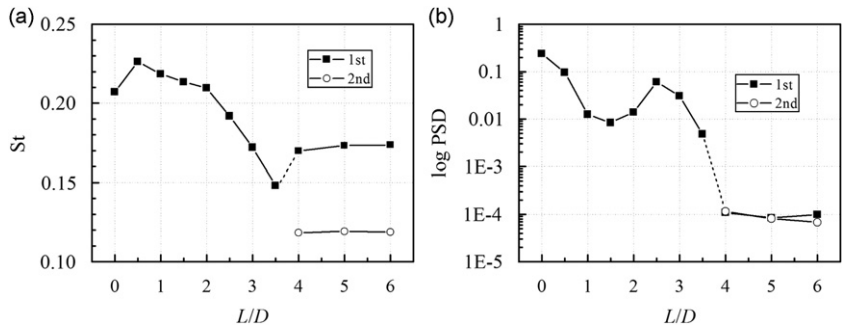

Fig. 18. The variation of Strouhal number: (a) St versus L/D; (b) The corresponding log PSD of St versus L/D. Key: ■, first peak frequency; ○, second peak frequency.

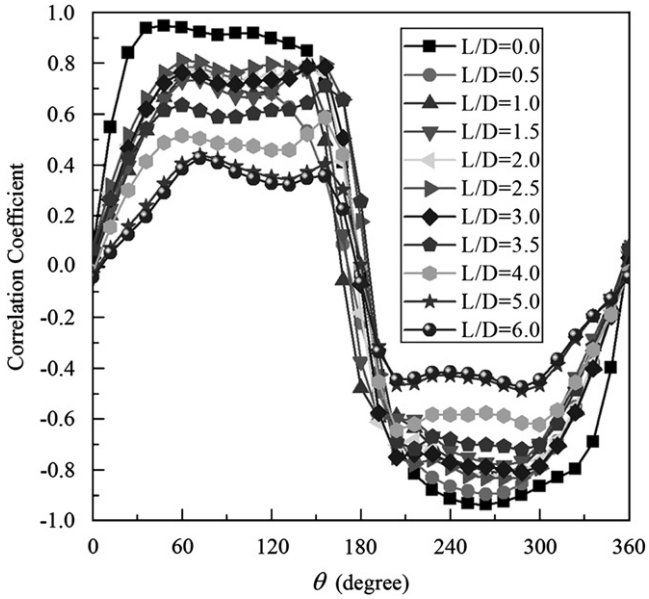

Fig. 19. The correlation of fluctuating lift and pressures on circumferential surface of the cylinder ($\tilde{R}_{lp(\theta)}$).

Correlation analysis requires synchronism between the signals which can be provided by the simultaneous multi-pressure measurement system used in this work.

The $\tilde{R}_{lp(\theta)}$ of all plates are plotted in Fig. 19. For bare cylinder and the long splitter plates ($L/D \geq 4.0$), the result is almost antisymmetric to $\theta=180^\circ$. But for the short splitter plates ($L/D \leq 3.5$), the absolute value of $\tilde{R}_{lp(\theta)}$ on side B is higher than side A. It proves that vortex on no-plate side develops more fully owing to more space. Besides, the correlation coefficient distributions of side A are similar to the long plates who has a turning point around $\theta=60^\circ$ while that of side B are similar to bare cylinder whose correlation coefficients from $\theta=200^\circ$ to 300° are close. Correlation coefficient of $L/D=2.5$ on side A is the highest, as well as $L/D=0.5$ on side B. Refer to Fig. 16, it is evident that higher absolute value of $\tilde{R}_{lp(\theta)}$ at $\theta=60^\circ\sim160^\circ$ and $\theta=200^\circ\sim300^\circ$causes higher C_l'.

Though the two separation points are not symmetrical for rotatable splitter plates, the $\tilde{R}_{p(s_A)p(\theta)}$ and $\tilde{R}_{p(s_B)p(\theta)}$ are very similar. Fig. 20 shows the $\tilde{R}_{p(s_B)p(\theta)}$ of all splitter plates where $p(s_B)$ means fluctuating pressure at $\theta=276^\circ$ (separation point on side B). The results show that the correlation coefficients from $\theta=200^\circ\sim300^\circ$ are close to 1 for all lengths plates which illustrates that the fluctuating pressures on the same side are synchronous. For the opposite side, the correlation coefficients vary a lot with the increase of L/D. The correlation coefficients of the two separation points $\tilde{R}_{p(s_B)p(s_A)}$ of all splitter plates are presented in Fig. 21. $\tilde{R}_{p(s_B)p(s_A)} \approx 0$ when $L/D=3.5$, which indicates the communication between the two shear layers is almost inhibited entirely. For $L/D<3.5$, there is a significant negative correlation between the pressures of the two separation points, indicating there are still two sets of alternating vortices on the two sides in spite of the inhibition caused by splitter plates. But different results were obtained for $L/D>3.5$, positive correlation shows that no alternating vortices developed in the near wake. It is not clear why there is positive correlation instead of no correlation between the pressures of the two sides. It is probably caused by the similarity between development of the shear layers on either side rather than the communication of the two shear layers.

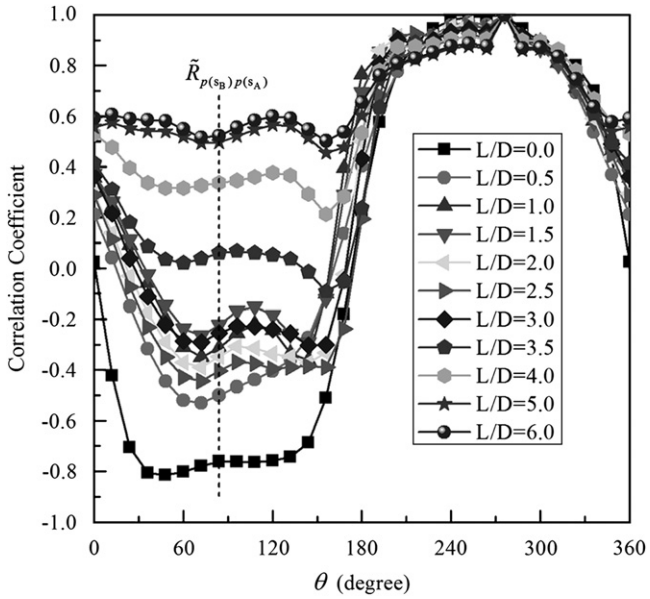

Fig. 20. The correlation of pressure at separation point and fluctuating pressures on circumferential surface of the cylinder ($\tilde{R}_{p(s_B)p(\theta)}$).

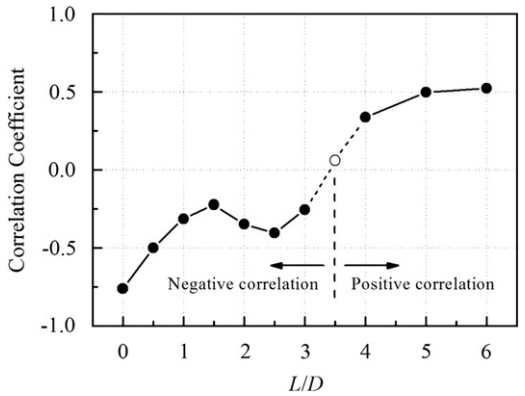

Fig. 21. The correlation coefficients of the two separation points $\tilde{R}_{p(s_B)p(s_A)}$.

3.6. Flow visualization

The smoke flow visualization technique is employed to help explain the differences in fluctuating forces by studying detailed flow structures. The center of the circular cylinder was chosen as the origin of the coordinate system. In order to clarify vortex generation, development and shedding process, the testing region was selected as 200×160 mm; with full 1024×1024-pixels image resolution and 2000 fps imaging speed. As a result of a light block caused by the splitter plate, there are dark areas on one side in the visualized images.

The visualized flow structures of the wake for bare circular cylinder and attaching fixed and rotatable splitter plates ($L/D=1.0$, $L/D=2.0$, and $L/D=4.0$) at $Re=4\times10^4$ are shown in Fig. 22. For the bare cylinder, there is a pair of alternating vortices generated from the two shear layers, which is in good agreement with previous studies. Fig. 22(c) and (e) show that the wakes of short rotatable plates are not grossly different from that of the bare cylinder. There are still obvious alternating vortices in the wake. When the splitter plate is fixed (Fig. 22(b) and (d)), however, the wake is altered significantly. Moreover, the fixed splitter plate forces an obvious delay in vortex formation. Thus the pressures near the cylinder are less affected by vortices. As mentioned above, for short rotatable splitter plates, the flow reattaches on to the tip of the plate on the side to which the plate deflected. And this seems to have the effect of stabilizing the near wake flow. The reattachment also results in a low pressure region between the separating shear layer and the plate, which leads to low pressure acting on the cylinder on the side to which the plate deflected. Besides, vortex shedding was visible downstream but this did not feed back to cause motion of the plate. Assi et al. (2009) also observed similar results in their vorticity contours.

But for long splitter plates, the flow structures of the fixed and the rotatable plates are nearly the same. Fig. 22(f) and (g) give an example for the case $L/D=4.0$. There is no flow reattachment taking place on either side of the plate and this is in

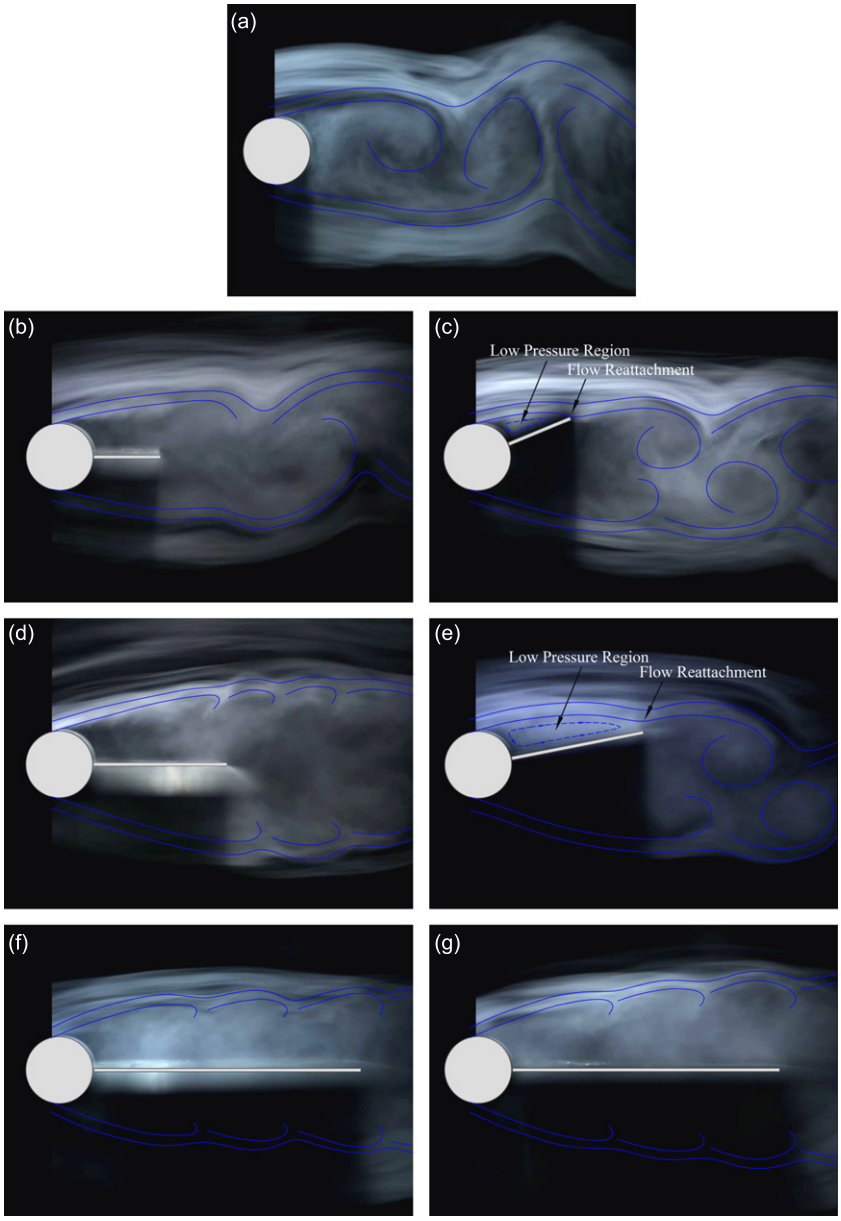

Fig. 22. The visualized flow structures of the wake at $Re=4\times10^4$: (a) Bare circular cylinder; (b) Fixed splitter plate ($L/D=1.0$); (c) Rotatable splitter plate ($L/D=1.0$); (d) Fixed splitter plate ($L/D=2.0$); (e) Rotatable splitter plate ($L/D=2.0$); (f) Fixed splitter plate ($L/D=4.0$); (g) Rotatable splitter plate ($L/D=4.0$).

good agreement with the results of pressure distribution. The communication between the two shear layers is totally inhibited that no large-scale vortices are generated.

As mentioned above, Gerrard (1966) declares that the frequency of vortex shedding is inversely proportional to the length scale of the vortex formation region immediately downstream of the body. He verified this suggestion for the case of a splitter plate forced to remain aligned with the flow. Further measurements by Bearman (1965) supported Gerrard (1966)'s explanation. As the present flow visualizations indicate, the vortex formation length scale of the short rotatable plate increases with L/D. And Fig. 18(a) shows the shedding frequency decreases with increasing L/D from 0.5 to 3.5. The explanation of vortex shedding suggested by Gerrard (1966) applies to the present rotatable splitter plate case as well.

4. Conclusions

The aerodynamic and flow characteristics of a circular cylinder with attached freely rotatable splitter plates with ratios of length to cylinder diameter (L/D) from 0.5 to 6.0 have been investigated experimentally. Measurements of the simultaneous circumferential pressure distribution, fluctuating forces and smoke flow visualization are presented.

It is verified that the splitter plates rotate to an off-axis equilibrium angle δ (on either side of the wake with equal probability) rather than align themselves with the free stream due to the integrated effect of the pressure difference along the sides of the splitter plates, until the pressure on both sides of the plate is balanced. The plate length L/D is crucial in determining the equilibrium angle δ. Longer splitter plate causes smaller angle; δ remains zero, i.e., parallel to the flow direction, for $L/D \geq 4$. The results are in good agreement with those findings from Cimbala and Garg (1991) and Assi et al. (2009).

The mean pressures in the wake near the cylinder are higher than that of the bare cylinder. The mean drag coefficients and the root-mean-square fluctuating lift coefficients, both largely determined by δ, are less than the corresponding bare cylinder; with a reduction up to about 30% and 90%, respectively. The shedding frequency is higher than bare cylinder when $L/D \leq 2$ but becomes lower than that when $L/D > 2$. St decreases from 0.226 to 0.148 with increasing L/D from 0.5 to 3.5. Due to the different equilibrium situation, St rises up to about 0.17 suddenly between $L/D=3.5$ and 4.0, and a second peak frequency appears.

Results of correlation analysis show that $\tilde{R}_{p(s_B)p(s_A)} \approx 0$ when $L/D=3.5$. For $L/D < 3.5$, there is a significant negative correlation between the pressures of the two separation points. But different results were obtained for $L/D > 3.5$, positive correlation shows that no alternating vortices developed in the near wake.

Finally, the visualized flow structures show that the wakes of short rotatable plates are not grossly different from that of the bare cylinder. There are still obvious alternating vortices in the wake. When fixed, however, the splitter plates significantly alter the wakes. For short rotatable splitter plates, the flow reattaches on to the tip of the plate on the side to which the plate deflected. But for long splitter plates, the flow structures of the fixed and the rotatable plates are nearly the same and there is no flow reattachment on either side of the plate.

Acknowledgments

The authors are grateful to the financial support from the National High Technology Research and Development Program of China (Grant No. 2008AA09Z310) and the National of Science Foundation of China (Grant No. 51079084). The authors are also grateful to the reviewers for their helpful comments to improve this paper.

Appendix A. Supplementary materials

Supplementary data associated with this article can be found in the online version at doi:10.1016/j.jfluidstructs.2011.11.005.

References

Akilli, H., Sahin, B., Tumen, N.F., 2005. Suppression of vortex shedding of circular cylinder in shallow water by a splitter plate. Flow Measurement and Instrumentation 16, 211–219.
Apelt, C.J., West, G.S., 1975. Effects of wake splitter plates on bluff-body flow in range $10^4 < \mathrm{Re} < 5 \times 10^4$. Journal of Fluid Mechanics 71, 145–160.
Apelt, C.J., West, G.S., Szewczyk, A.A., 1973. Effects of wake splitter plates on flow past a circular cylinder in range $10^4 < \mathrm{Re} < 5 \times 10^4$. Journal of Fluid Mechanics 61, 187–198.
Assi, G.R.S., Bearman, P.W., Kitney, N., 2009. Low drag solutions for suppressing vortex-induced vibration of circular cylinders. Journal of Fluids and Structures 25, 666–675.
Assi, G.R.S., Bearman, P.W., Kitney, N., Tognarelli, M.A., 2010. Suppression of wake-induced vibration of tandem cylinders with free-to-rotate control plates. Journal of Fluids and Structures 26, 1045–1057.
Baarholm, G.S., Larsen, C.M., Lie, H., 2005. Reduction of VIV using suppression devices – An empirical approach. Marine Structures 18, 489–510.
Bearman, P.W., 1965. Investigation of the flow behind a two-dimensional model with a blunt trailing edge and fitted with splitter plates. Journal of Fluid Mechanics 21, 241–255.
Cantwell, B., Coles, D., 1983. An experimental study of entrainment and transport in the turbulent near wake of a circular cylinder. Journal of Fluid Mechanics 136, 321–374.
Cimbala, J.M., Garg, S., 1991. Flow in the wake of a freely rotatable cylinder with splitter plate. AIAA Journal 29, 1001–1003.
Fage, A., Falkner, V.M., 1931. Further experiments on the flow around a circular cylinder. Reports and Memoranda of the Aeronautical Research Council (London), R&M 1369, 1–13.
Fox, T.A., West, G.S., 1990. On the use of end plates with circular cylinders. Experiments in Fluids 9, 237–239.
Gerrard, J.H., 1954. A disturbance-sensitive Reynolds number range of the flow past a circular cylinder. Journal of Fluid Mechanics 22, 187–196.
Gerrard, J.H., 1966. The mechanics of the formation region of vortices behind bluff bodies. Journal of Fluid Mechanics 25, 401–413.
Gu, F., Wang, J.S., Zhong, Q., Qiao, X.Q., Huang, Z., 2009. Wind tunnel test of VIV control on marine riser with splitter plates, The 9th National Congress on Hydrodynamics and 22nd National Conference on Hydrodynamics, Chengdu, China (in Chinese), pp. 481–487.
Huang, S., 2011. VIV suppression of a two-degree-of-freedom circular cylinder and drag reduction of a fixed circular cylinder by the use of helical grooves. Journal of Fluids and Structures 27, 1124–1133.
Irwin, H.P.A.H., Cooper, K.R., Girard, R., 1979. Correction of distortion effects caused by tubing systems in measurements of flucuating pressures. Journal of Wind Engineering and Industrial Aerodynamics 5, 93–107.
Korkischko, I., Meneghini, J.R., 2010. Experimental investigation of flow-induced vibration on isolated and tandem circular cylinders fitted with strakes. Journal of Fluids and Structures 26, 611–625.
Lam, K., Lin, Y.F., Zou, L., Liu, Y., 2010. Investigation of turbulent flow past a yawed wavy cylinder. Journal of Fluids and Structures 26, 1078–1097.
Lam, K., Wang, F.H., Li, J.Y., So, R.M.C., 2004. Experimental investigation of the mean and fluctuating forces of wavy (varicose) cylinders in a cross-flow. Journal of Fluids and Structures 19, 321–334.

Nishimura, H., Taniike, Y., 2001. Aerodynamic characteristics of fluctuating forces on a circular cylinder. Journal of Wind Engineering and Industrial Aerodynamics 89, 713–723.
Norberg, C., 2003. Fluctuating lift on a circular cylinder: review and new measurements. Journal of Fluids and Structures 17, 57–96.
Roshko, A., 1953. On the Development of Turbulent Wakes from Vortex Street. NACA Technical Note 2913.
Shukla, S., Govardhan, R.N., Arakeri, J.H., 2009. Flow over a cylinder with a hinged-splitter plate. Journal of Fluids and Structures 25, 713–720.
Szepessy, S., Bearman, P.W., 1992. Aspect ratio and end plate effects on vortex shedding from a circular cylinder. Journal of Fluid Mechanics 234, 191–217.
Texier, A., Bustamante, A.S.C., David, L., 2002. Contribution of a short separating plate on the control of the swirling process downstream a half-cylinder. Experimental Thermal and Fluid Science 26, 565–572.
Unal, M.F., Rockwell, D., 1988. On vortex formation from a cylinder. Part 2. Control by splitter-plate interference. Journal of Fluid Mechanics 190, 513–529.
Wang, J.S., Jiang, S.Q., Tan, B., Gu, F., 2009. Numerical simulation of flow control on marine riser with attached splitter plates at Reynolds number of 1000 and 10000, CSHydro 2009 Conference, Keelung, Taiwan (in Chinese).
Wang, J.S., Liu, H., Gu, F., Zhao, P.L., 2010. Numerical simulation of flow control on marine riser with attached splitter plate, 29th International Conference on Ocean, Offshore and Artic Engineering, Shanghai, China, pp. 489–498.
Weidman, P.D., 1968. Wake transiton and blockage effects on cylinder base pressures. Ph. D. Thesis, California Institute of Technology, Pasadena, California.
Wieselsberger, C., 1921. Neuere Feststellungen Uber die Gesetze des Flussigkeits.und Luftwiderstands. Physikalische Zeitschrift 22, 321–328.
Zdravkovich, M.M., 1981. Review and classification of various aerodynamic and hydrodynamic means for suppressing vortex shedding. Journal of Wind Engineering and Industrial Aerodynamics 7, 145–189.
Zdravkovich, M.M., 1997. Flow around Circular Cylinders, Vol. 1: Fundamentals. Oxford Science Publications, Oxford.